



Article

# A Challenge toward Novel Quaternary Sulfides $\text{SrLnCuS}_3$ (Ln = La, Nd, Tm): Unraveling Synthetic Pathways, Structures and Properties

Anna V. Ruseikina <sup>1</sup>, Maxim V. Grigoriev <sup>1</sup>, Leonid A. Solovyov <sup>2</sup>, Vladimir A. Chernyshev <sup>3</sup>, Aleksandr S. Aleksandrovsky <sup>4,5</sup>, Alexander S. Krylov <sup>4</sup>, Svetlana N. Krylova <sup>4</sup>, Nikolai P. Shestakov <sup>4</sup>, Dmitriy A. Velikanov <sup>4</sup>, Alexander A. Garmonov <sup>6</sup>, Alexey V. Matigrov <sup>1</sup>, Marcel A. Eberle <sup>7</sup>, Thomas Schleid <sup>7</sup> and Damir A. Safin <sup>8,9,10,\*</sup>

- <sup>1</sup> Laboratory of Theory and Optimization of Chemical and Technological Processes, University of Tyumen, 625003 Tyumen, Russia
  - <sup>2</sup> Federal Research Center KSC SB RAS, Institute of Chemistry and Chemical Technology, 660036 Krasnoyarsk, Russia
  - <sup>3</sup> Institute of Natural Sciences and Mathematics, Ural Federal University named after the First President of Russia B.N. Yeltsin, Mira Str. 19, 620002 Ekaterinburg, Russia
  - <sup>4</sup> Kirensky Institute of Physics, Federal Research Center KSC SB RAS, 660036 Krasnoyarsk, Russia
  - <sup>5</sup> Department of Photonics and Laser Technology, Siberian Federal University, 660079 Krasnoyarsk, Russia
  - <sup>6</sup> Institute of Physics and Technology, University of Tyumen, Volodarskogo Str. 6, 625003 Tyumen, Russia
  - <sup>7</sup> Institute of Inorganic Chemistry, University of Stuttgart, D-70569 Stuttgart, Germany
  - <sup>8</sup> Scientific and Educational Center for Chemical and Pharmaceutical Technologies, Ural Federal University named after the First President of Russia B.N. Yeltsin, Mira Str. 19, 620002 Ekaterinburg, Russia
  - <sup>9</sup> «Advanced Materials for Industry and Biomedicine» Laboratory, Kurgan State University, Sovetskaya Str. 63/4, 640020 Kurgan, Russia
  - <sup>10</sup> University of Tyumen, Volodarskogo Str. 6, 625003 Tyumen, Russia
- \* Correspondence: damir.a.safin@gmail.com



**Citation:** Ruseikina, A.V.; Grigoriev, M.V.; Solovyov, L.A.; Chernyshev, V.A.; Aleksandrovsky, A.S.; Krylov, A.S.; Krylova, S.N.; Shestakov, N.P.; Velikanov, D.A.; Garmonov, A.A.; et al. A Challenge toward Novel Quaternary Sulfides  $\text{SrLnCuS}_3$  (Ln = La, Nd, Tm): Unraveling Synthetic Pathways, Structures and Properties. *Int. J. Mol. Sci.* **2022**, *23*, 12438. <https://doi.org/10.3390/ijms232012438>

Academic Editor: Andreas Taubert

Received: 27 September 2022

Accepted: 10 October 2022

Published: 18 October 2022

**Publisher's Note:** MDPI stays neutral with regard to jurisdictional claims in published maps and institutional affiliations.



**Copyright:** © 2022 by the authors. Licensee MDPI, Basel, Switzerland. This article is an open access article distributed under the terms and conditions of the Creative Commons Attribution (CC BY) license (<https://creativecommons.org/licenses/by/4.0/>).

**Abstract:** We report on the novel heterometallic quaternary sulfides  $\text{SrLnCuS}_3$  (Ln = La, Nd, Tm), obtained as both single crystals and powdered samples. The structures of both the single crystal and powdered samples of  $\text{SrLaCuS}_3$  and  $\text{SrNdCuS}_3$  belong to the orthorhombic space group  $Pnma$  but are of different structural types, while both samples of  $\text{SrTmCuS}_3$  crystallize in the orthorhombic space group  $Cmcm$  with the structural type  $\text{KZrCuS}_3$ . Three-dimensional crystal structures of  $\text{SrLaCuS}_3$  and  $\text{SrNdCuS}_3$  are formed from the (Sr/Ln) $\text{S}_7$  capped trigonal prisms and  $\text{CuS}_4$  tetrahedra. In  $\text{SrLaCuS}_3$ , alternating 2D layers are stacked, while the main backbone of the structure of  $\text{SrNdCuS}_3$  is a polymeric 3D framework  $[(\text{Sr/Ln})\text{S}_7]_n$ , strengthened by 1D polymeric chains  $(\text{CuS}_4)_n$  with 1D channels, filled by the other  $\text{Sr}^{2+}/\text{Ln}^{3+}$  cations, which, in turn, form 1D dimeric ribbons. A 3D crystal structure of  $\text{SrTmCuS}_3$  is constructed from the  $\text{SrS}_6$  trigonal prisms,  $\text{TmS}_6$  octahedra and  $\text{CuS}_4$  tetrahedra. The latter two polyhedra are packed together into 2D layers, which are separated by 1D chains  $(\text{SrS}_6)_n$  and 1D free channels. In both crystal structures of  $\text{SrLaCuS}_3$  obtained in this work, the crystallographic positions of strontium and lanthanum were partially mixed, while only in the structure of  $\text{SrNdCuS}_3$ , solved from the powder X-ray diffraction data, were the crystallographic positions of strontium and neodymium partially mixed. Band gaps of  $\text{SrLnCuS}_3$  (Ln = La, Nd, Tm) were found to be 1.86, 1.94 and 2.57 eV, respectively. Both  $\text{SrNdCuS}_3$  and  $\text{SrTmCuS}_3$  were found to be paramagnetic at 20–300 K, with the experimental magnetic characteristics being in good agreement with the corresponding calculated parameters.

**Keywords:** inorganic materials; quaternary sulfide; synthesis; crystal structure; ab initio calculations; magnetic measurements; spectroscopy

## 1. Introduction

Layered chalcogenides containing *d*-metals are of particular interest due to their valuable properties, as well as being used as superconductors [1], magnetic [2,3] and thermoelectric materials [4], materials for infrared and nonlinear optics [5–7] and catalysts [8]. The quaternary chalcogenides  $ABCX_3$  (A is an alkali or alkaline earth metal, Eu; B is a *d*- or *f*-element; C is a *d*-element; X is a chalcogenide) produce layered and/or channel structures, crystallizing in various structural types [9–23]. An overwhelming majority of the crystal structures of  $ABCX_3$  exhibit 2D anionic layers  $[BCX_3]^{n-}$  with trapped  $A^{n+}$  cations. Both the nature and charge of  $A^{n+}$  affect the lattice distortion, electronic structure, phonon dispersion, electrical properties, and heat transfer properties in the crystal structure [24].  $ABCX_3$  compounds exhibit very low lattice thermal conductivity [25–27], promising thermoelectric characteristics [24,28] and high photovoltaic efficiency [27]. Thus, thermodynamically stable quaternary compounds are potential high-performance thermoelectrics, thermal barrier coatings, and thermal data-storage devices [26,29–32]. Furthermore, semiconductor, magnetic, optical, and thermodynamic properties have also been described for these compounds [4,9–20,23,24,33–38].

Of the  $ABCX_3$  compounds, the quaternary chalcogenides  $ALnCuX_3$  are of particular interest, since transition and rare earth elements exhibit rich crystal chemistry and specific spectroscopic properties. According to quantum mechanical calculations, the band gap of  $SrLnCuS_3$  is 1.00–1.51 eV [26], indicating that these compounds are promising materials for solar cells with an efficiency of about 20% [39–42]. However, the lack of experimental data on the band gap of  $SrLnCuS_3$  limits their practical utilization.

Polycrystalline samples of  $SrLnCuS_3$  were obtained by the melting of a stoichiometric ratio of sulfides  $SrS$ ,  $Ln_2S_3$  and  $Cu_2S$ , followed by annealing at 970–1170 K for 2–3 (!) months [22,34–36,43–45]. Single-crystal samples were synthesized from elemental Sr, Cu and Ln (Ln = Nd, Y, Sc) using a halide flux at 1070 K for 8 days [46,47]. Recently, we have reported on the synthesis of  $EuLnCuS_3$  by the sulfidation of a mixture of oxides obtained by thermolysis of co-crystallized copper nitrate and rare-earth nitrates for 25 h [48]. Thus, using this approach would, likely, significantly reduce the synthesis time towards  $SrLnCuS_3$ . Notably, strontium oxide is more active than europium oxide with respect to the material of the reactor used for synthesis due to the presence of an alkaline earth element. Therefore, it is suggested that the initial synthesis temperatures to produce  $SrLnCuS_3$  should be lower than those of  $EuLnCuS_3$ .

In the literature, the crystal structures of some  $SrLnCuS_3$  have already been reported [21,22,34–36,43–47]. For  $SrLnCuS_3$ , two types of orthorhombic crystal structures with *Pnma* symmetry and one type with *Cmcm* symmetry were revealed [22]. Sulfides  $SrLnCuS_3$  (Ln = La–Nd) crystallize in the  $BaLaCuS_3$  structural type, and the crystallographic positions of the  $Sr^{2+}$  and  $Ln^{3+}$  ions are partially mixed by 21% in  $SrLaCuS_3$  [22,43], by 16% in  $SrCeCuS_3$  [44] and by 11% in  $SrPrCuS_3$  [22,43], while in  $SrNdCuS_3$  the  $Sr^{2+}$  and  $Ln^{3+}$  cations occupy two different crystallographic positions [46]. It should also be noted that, for  $SrNdCuS_3$ , the second modification of the structural type  $Eu_2CuS_3$  was obtained [46], while for  $SrCeCuS_3$ , a high-temperature polymorphic modification of the structural type  $Ba_2MnS_3$  with a partially mixed crystallographic positions of the  $Sr^{2+}$  and  $Ce^{3+}$  ions was also revealed [44].

The isostructural quaternary sulfides  $EuLnCuS_3$  [37,49] and selenides  $EuLnCuSe_3$  [23] and  $SrLnCuSe_3$  [50,51] always start to crystallize in the structural type  $Ba_2MnS_3$ . Due to the similar ionic radii of  $Eu^{2+}$  and  $Sr^{2+}$  (1.17 and 1.18 Å, respectively [52]), the structural types of  $EuLnCuS_3$  and  $SrLnCuS_3$  should also be similar. Thus, it can tentatively be assumed that  $SrLaCuS_3$  will also crystallize in the structural type  $Ba_2MnS_3$ . Sulfides  $SrLnCuS_3$  (Ln = Sm [22], Gd [22], Ho [35], Y [47]) belong to the structural type  $Eu_2CuS_3$ , while  $SrLnCuS_3$  (Ln = Er [45], Yb [45], Lu [22], Sc [36]) are of the structural type  $KZrCuS_3$ . In all the listed compounds, the  $Eu^{2+}$  and  $Ln^{3+}$  ions occupy two crystallographically independent positions. The change of space group from *Pnma* to *Cmcm* occurs between  $SrYCuS_3$  and  $SrErCuS_3$  [23].  $SrLnCuS_3$  melt incongruently at 1429–1712 K [34,43].  $SrLaCuS_3$

and SrPrCuS<sub>3</sub> are optically transparent in the IR range from 1800 to 3600 cm<sup>-1</sup> [43]. To the best of our knowledge, other physical properties of sulfides SrLnCuS<sub>3</sub> have not been reported so far.

With all this in mind, in this work we have focused on the synthesis of SrLnCuS<sub>3</sub> (Ln = La, Nd, Tm), as well as studying their crystal structures, magnetic and optical properties.

## 2. Results and Discussion

The heterometallic quaternary sulfides SrLnCuS<sub>3</sub> (Ln = La, Nd, Tm) were obtained both in the form of single crystals as well as powdered samples. The former synthetic procedure requires heating a stoichiometric ratio of the elements Sr, Cu, Ln and S in the presence of CsBr as a flux for 8 days at 1070 K, while the latter synthetic approach significantly decreases the reaction time in comparison to both a single-crystal method and the sulfide-melting method [22,35,43–45,47].

To date, for the quaternary sulfides, only four crystal structures of SrLnCuS<sub>3</sub> (Ln = Nd, Y, Sc), solved from the single-crystal X-ray diffraction data, have been known so far (Table 1) [46,47], while twelve crystal structures of a series of SrLnCuS<sub>3</sub> (Ln = La, Ce, Pr, Nd, Sm, Gd, Ho, Er, Tm, Yb, Lu, Sc), solved from the powder X-ray diffraction data, have been reported (Table 2) [22,36,44,45].

**Table 1.** Experimental details for the structures of SrLnCuS<sub>3</sub>, solved from the single-crystal X-ray diffraction data.

	SrLaCuS <sub>3</sub> <sup>a</sup>	SrNdCuS <sub>3</sub> <sup>a</sup>	SrNdCuS <sub>3</sub> <sup>a</sup>	SrYCuS <sub>3</sub> <sup>a</sup>	SrTmCuS <sub>3</sub> <sup>a</sup>	SrScCuS <sub>3</sub> <sup>a</sup>
Space group	<i>Pnma</i>	<i>Pnma</i>	<i>Pnma</i>	<i>Pnma</i>	<i>Cmcm</i>	<i>Cmcm</i>
Structural type	Ba <sub>2</sub> MnS <sub>3</sub>	BaLaCuS <sub>3</sub>	Eu <sub>2</sub> CuS <sub>3</sub>	Eu <sub>2</sub> CuS <sub>3</sub>	KZrCuS <sub>3</sub>	KZrCuS <sub>3</sub>
<i>a</i> (Å)	8.1682(6)	11.0663(8)	10.5693(7)	10.1845(7)	3.9163(3)	3.8316(3)
<i>b</i> (Å)	4.0748(3)	4.0886(3)	4.0072(3)	3.9378(3)	12.9520(9)	12.8504(9)
<i>c</i> (Å)	16.0394(11)	11.4625(8)	12.8905(9)	12.9426(9)	10.0642(7)	9.7153(7)
<i>V</i> (Å <sup>3</sup> )	533.85(7)	518.63(2)	545.96(3)	519.06(2)	510.50(6)	478.36(2)
<i>Z</i>	4	4	4	4	4	4
$\rho$ (g cm <sup>-3</sup> )	4.806	5.015	4.764	4.303	5.416	4.059
$\mu$ (mm <sup>-1</sup> )	22.76	25.20	23.94	26.41	32.81	18.01
Collected reflection	13821	7074	10117	8491	2756	4498
Unique reflections	846	678	738	734	340	351
<i>R</i> <sub>int</sub>	0.0653	0.068	0.137	0.075	0.0678	0.055
<i>R</i> <sub>1</sub> (all)	0.0217	0.032	0.043	0.029	0.0248	0.017
<i>wR</i> <sub>2</sub> (all)	0.0382	0.054	0.080	0.033	0.0426	0.032
<i>S</i>	1.022	1.059	1.004	0.941	1.007	1.031
Reference	This work	[46]	[46]	[47]	This work	[47]

<sup>a</sup> Heating a stoichiometric ratio of the elements Sr, Ln, Cu and S in the presence of CsBr as a flux in an evacuated quartz ampoule for 8 days at 1070–1120 K.

In the present work, we report for the first time the crystal structures of SrLaCuS<sub>3</sub> and SrTmCuS<sub>3</sub> (Table 1), solved from the single-crystal X-ray diffraction data, as well as the crystal structure of SrLnCuS<sub>3</sub> (Ln = La, Nd, Tm), solved from the powder X-ray diffraction data (Table 2). Notably, the same synthetic approach for the formation of single crystals yields one structural type, Ba<sub>2</sub>MnS<sub>3</sub>, for SrLaCuS<sub>3</sub>, and two structural types, BaLaCuS<sub>3</sub> and Eu<sub>2</sub>CuS<sub>3</sub>, for SrNdCuS<sub>3</sub> of the orthorhombic space group *Pnma*, while for SrTmCuS<sub>3</sub>, the structural type KZrCuS<sub>3</sub> of the orthorhombic space group *Cmcm* was established (Table 1). However, different synthetic approaches toward powdered samples yield two structural types, BaLaCuS<sub>3</sub> and Ba<sub>2</sub>MnS<sub>3</sub>, for SrLaCuS<sub>3</sub>, one structural type, BaLaCuS<sub>3</sub>, for SrNdCuS<sub>3</sub> of the same orthorhombic space group *Pnma*, and one structural type, KZrCuS<sub>3</sub>, of the orthorhombic space group *Cmcm* for SrTmCuS<sub>3</sub> (Table 2). Interestingly, while the *b* axis in the structures of SrLaCuS<sub>3</sub> and SrNdCuS<sub>3</sub> is very similar and varies from 4.0072(3) Å to 4.11053(6) Å, the *a* and *c* axes differ significantly ranging from 8.1682(6) Å to 16.0394(11) Å

(Tables 1 and 2). Furthermore, the cell volume is almost the same in the structures of SrLaCuS<sub>3</sub>, regardless of the structural type, and of 533.85(7)–535.97(1) Å<sup>3</sup>, but differs in the structures of SrNdCuS<sub>3</sub>. Particularly, the cell volume is 518.63(2)–519.14(1) Å<sup>3</sup> in the structural type BaLaCuS<sub>3</sub>, and is remarkably larger in the structural type Eu<sub>2</sub>CuS<sub>3</sub> (545.96(3) Å<sup>3</sup>). The cell volume in the structures of SrLaCuS<sub>3</sub> is smaller and of 510.50(6)–511.34(3) Å<sup>3</sup>.

**Table 2.** Experimental details for the structures of SrLnCuS<sub>3</sub>, solved from the powder X-ray diffraction data.

	SrLaCuS <sub>3</sub> <sup>a</sup>	SrLaCuS <sub>3</sub> <sup>b</sup>	SrCeCuS <sub>3</sub> <sup>a</sup>	SrCeCuS <sub>3</sub> <sup>c</sup>	SrPrCuS <sub>3</sub> <sup>a</sup>	SrNdCuS <sub>3</sub> <sup>d</sup>	SrSmCuS <sub>3</sub> <sup>a</sup>
Space group	<i>Pnma</i>	<i>Pnma</i>	<i>Pnma</i>	<i>Pnma</i>	<i>Pnma</i>	<i>Pnma</i>	<i>Pnma</i>
Structural type	BaLaCuS <sub>3</sub>	Ba <sub>2</sub> MnS <sub>3</sub>	BaLaCuS <sub>3</sub>	Ba <sub>2</sub> MnS <sub>3</sub>	BaLaCuS <sub>3</sub>	BaLaCuS <sub>3</sub>	Eu <sub>2</sub> CuS <sub>3</sub>
<i>a</i> (Å)	11.2415(1)	8.1746(3)	11.1626(2)	8.1393(3)	11.1171(1)	11.0815(2)	10.4285(2)
<i>b</i> (Å)	4.11053(6)	4.0727(2)	4.0970(2)	4.0587(2)	4.09492(6)	4.0849(1)	3.98640(7)
<i>c</i> (Å)	11.5990(1)	16.0473(8)	11.5307(1)	15.9661(2)	11.5069(2)	11.4684(2)	12.9325(2)
<i>V</i> (Å <sup>3</sup> )	535.97(1)	534.26(4)	527.33(1)	527.44(2)	523.84(1)	519.14(1)	537.63(2)
<i>R</i> <sub>DDM</sub> (%)	5.25	5.73	4.52	6.61	5.03	4.00	4.94
<i>R</i> <sub>F</sub> (%)	1.53	1.1	2.87	3.78	1.80	3.7	2.09
Impurity	–	2.6% SrS	–	–	–	5.2% SrS 1.3% NdCuSO	2.6% SmCuS <sub>2</sub> 1.6% Sm <sub>2</sub> SO <sub>2</sub>
Reference	[43]	This work	[44]	[44]	[43]	This work	[22]
	SrGdCuS <sub>3</sub> <sup>a</sup>	SrHoCuS <sub>3</sub> <sup>c</sup>	SrErCuS <sub>3</sub> <sup>a</sup>	SrErCuS <sub>3</sub> <sup>c</sup>	SrTmCuS <sub>3</sub> <sup>e</sup>	SrYbCuS <sub>3</sub> <sup>c</sup>	SrLuCuS <sub>3</sub> <sup>a</sup>
Space group	<i>Pnma</i>	<i>Pnma</i>	<i>Cmcm</i>	<i>Cmcm</i>	<i>Cmcm</i>	<i>Cmcm</i>	<i>Cmcm</i>
Structural type	Eu <sub>2</sub> CuS <sub>3</sub>	Eu <sub>2</sub> CuS <sub>3</sub>	KZrCuS <sub>3</sub>	KZrCuS <sub>3</sub>	KZrCuS <sub>3</sub>	KZrCuS <sub>3</sub>	KZrCuS <sub>3</sub>
<i>a</i> (Å)	10.3288(2)	10.1487(1)	3.92672(5)	3.93128(3)	3.9210(1)	3.91448(4)	3.91105(4)
<i>b</i> (Å)	3.96271(7)	3.9332(1)	12.9632(2)	12.9709(1)	12.9523(5)	12.9554(1)	12.9504(1)
<i>c</i> (Å)	12.9397(2)	12.9524(2)	10.0974(1)	10.1161(1)	10.0687(4)	10.0332(1)	10.0206(1)
<i>V</i> (Å <sup>3</sup> )	529.62(2)	517.02(2)	513.99(1)	515.843(9)	511.34(3)	508.842(8)	507.540(8)
<i>R</i> <sub>DDM</sub> (%)	4.41	4.29	5.67	3.73	4.80	3.56	5.27
<i>R</i> <sub>F</sub> (%)	2.18	1.91	2.60	2.06	2.60	1.48	1.27
Impurity	3.6% GdCuS <sub>2</sub> 2.5% SrS 0.8% Gd <sub>2</sub> SO <sub>2</sub>	2.6% SrS	6.3% Er <sub>x</sub> Cu <sub>y</sub> S <sub>2</sub> 3.5% SrS	9.5% Er <sub>2</sub> SO <sub>2</sub> 1.2% SrS 0.5% Er <sub>5</sub> S(SiO <sub>4</sub> ) <sub>3</sub>	5.1% Tm <sub>2</sub> SO <sub>2</sub> 1.2% SrS	2.2% Yb <sub>2</sub> SO <sub>2</sub> 1.8% Yb <sub>5</sub> S(SiO <sub>4</sub> ) <sub>3</sub> 1.2% SrS	1.6% SrS 1.1% Lu <sub>2</sub> SO <sub>2</sub>
Reference	[22]	[36]	[22]	[45]	This work	[45]	[22]

<sup>a</sup> Melting of sulfides Cu<sub>2</sub>S, Ln<sub>2</sub>S<sub>3</sub> and SrS under a high-frequency current condition, followed by annealing at 970 K for 3 months. <sup>b</sup> Sulfidation of oxides (Sr<sub>0.15</sub>La<sub>1.85</sub>)CuO<sub>4</sub>, (Sr<sub>0.05</sub>La<sub>1.95</sub>)CuO<sub>4</sub>, SrLnCuO<sub>4</sub> obtained by thermal decomposition of nitrates, at 1170 K. <sup>c</sup> Melting of sulfides Cu<sub>2</sub>S, Ln<sub>2</sub>S<sub>3</sub> and SrS under a high-frequency current condition, followed by annealing at 1170 K for 2 months. <sup>d</sup> Sulfidation of oxides Nd<sub>2</sub>O<sub>3</sub>, Sr<sub>2</sub>CuO<sub>4</sub> and Nd<sub>2</sub>CuO<sub>4</sub>, obtained by thermal decomposition of nitrates, at 1170 K. <sup>e</sup> Sulfidation of oxides SrTm<sub>2</sub>O<sub>4</sub>, Tm<sub>2</sub>O<sub>3</sub>, Sr<sub>2</sub>CuO<sub>4</sub>, Tm<sub>2</sub>CuO<sub>4</sub> and CuSrO<sub>2</sub>, obtained by thermal decomposition of nitrates, at 1170 K.

It should also be noted that in both crystal structures of SrLaCuS<sub>3</sub> obtained in this work, the crystallographic positions of strontium and lanthanum were partially mixed by about 50% and 45%, respectively, while only in the structure of SrNdCuS<sub>3</sub>, solved from the powder X-ray diffraction data, the crystallographic positions of strontium and neodymium were partially mixed by about 11% (Table 3). In both structures of SrTmCuS<sub>3</sub>, each atom fully occupies its own crystallographical position (Table 3).

A 3D crystal structure of both SrLaCuS<sub>3</sub> and SrNdCuS<sub>3</sub> was constructed from the (Sr1/Ln1)S<sub>7</sub>- and (Sr2/Ln2)S<sub>7</sub>-capped trigonal prisms as well as CuS<sub>4</sub> tetrahedra (Figure 1). However, different structural types of these compounds are clearly reflected in the packing of coordination polyhedra. Particularly, in the structure of SrLaCuS<sub>3</sub>, the (Sr1/La1)S<sub>7</sub>- and (Sr2/La2)S<sub>7</sub>-capped trigonal prisms each form alternating 2D layers, of which the (Sr1/La1)S<sub>7</sub>-based layers are further strengthened by 1D polymeric chains (CuS<sub>4</sub>)<sub>n</sub> (Figure 1). The main

backbone of the structure of SrNdCuS<sub>3</sub> is a polymeric 3D framework [(Sr1/Ln1)S<sub>7</sub>]<sub>n</sub>, further strengthened by 1D polymeric chains (CuS<sub>4</sub>)<sub>n</sub>, with 1D channels along the *b* axis, filled by the Sr<sup>2+</sup>/Ln<sup>3+</sup> cations, which, in turn, form 1D dimeric ribbons along the *b* axis (Figure 1). A 3D crystal structure of SrTmCuS<sub>3</sub> differs significantly from the La- and Nd-based derivatives and is constructed from the SrS<sub>6</sub> trigonal prisms and TmS<sub>6</sub> octahedra as well as CuS<sub>4</sub> tetrahedra (Figure 1). The latter two polyhedra are packed together into 2D layers, which are separated by 1D chains (SrS<sub>6</sub>)<sub>n</sub> and 1D free channels along the *a* axis (Figure 1).

**Table 3.** Fractional atomic coordinates and occupancy of SrLnCuS<sub>3</sub> (Ln = La, Nd, Tm).

Atom	<i>x</i>	<i>y</i>	<i>z</i>	Occupancy	<i>x</i>	<i>y</i>	<i>z</i>	Occupancy
SrLaCuS <sub>3</sub> (single crystal)				SrLaCuS <sub>3</sub> (powdered sample)				
Sr1	0.09058(3)	1/4	0.785319(17)	0.502(5)	0.09026(6)	1/4	0.785177(28)	0.5453(46)
La1	0.09058(3)	1/4	0.785319(17)	0.498(5)	0.09026(6)	1/4	0.785177(28)	0.4547(46)
Sr2	0.25439(3)	1/4	0.038345(17)	0.489(6)	0.25446(6)	1/4	0.038210(26)	0.4550(43)
La2	0.25439(3)	1/4	0.038345(17)	0.511(6)	0.25446(6)	1/4	0.038210(26)	0.5450(43)
Cu	0.11864(6)	1/4	0.36655(3)	1	0.11857(11)	1/4	0.36652(6)	1
S1	0.17928(12)	1/4	0.22120(6)	1	0.17956(18)	1/4	0.22114(9)	1
S2	0.38083(12)	1/4	0.42864(6)	1	0.38097(19)	1/4	0.42837(10)	1
S3	0.01190(12)	1/4	0.60039(6)	1	0.01197(18)	1/4	0.60006(10)	1
SrNdCuS <sub>3</sub> (single crystal) [46]				SrNdCuS <sub>3</sub> (powdered sample)				
Sr1	0.31732(6)	1/4	0.49523(6)	1	0.31752(15)	1/4	0.49500(17)	0.886(5)
Nd1	0.48946(3)	1/4	0.81684(4)	1	0.31752(15)	1/4	0.49500(17)	0.114(5)
Sr2	–	–	–	–	0.48947(13)	1/4	0.81683(11)	0.114(5)
Nd2	–	–	–	–	0.48947(13)	1/4	0.81683(11)	0.886(5)
Cu	0.24480(8)	1/4	0.21334(9)	1	0.2447(2)	1/4	0.2133(3)	1
S1	0.22363(17)	1/4	0.80669(16)	1	0.2250(5)	1/4	0.8076(4)	1
S2	0.04818(16)	1/4	0.14176(17)	1	0.0487(4)	1/4	0.1406(4)	1
S3	0.38733(17)	1/4	0.05848(17)	1	0.3872(4)	1/4	0.0571(4)	1
SrTmCuS <sub>3</sub> (single crystal)				SrTmCuS <sub>3</sub> (powdered sample)				
Sr	0	0.74817(7)	1/4	1	0	0.74800(12)	1/4	1
Tm	0	0	0	1	0	0	0	1
Cu	0	0.47124(9)	1/4	1	0	0.47147(17)	1/4	1
S1	0	0.36340(13)	0.06401(14)	1	0	0.3634(2)	0.0644(2)	1
S2	0	0.07621(18)	1/4	1	0	0.0761(3)	1/4	1

In the discussed structures of SrLaCuS<sub>3</sub>, the Sr/La–S bond lengths are 2.910(1)–3.09999(17) Å, while the Sr/Nd–S bonds in the structures of SrNdCuS<sub>3</sub> vary in a broader range from 2.843(1) Å to 3.136(2) Å (Table 4). The Sr–S bond lengths in the structures of SrTmCuS<sub>3</sub> are similar to those in the La- and Nd-based derivatives, and of 2.966(3)–3.093(2) Å, while the Tm–S bonds are shorter and of 2.703(2)–2.719(2) Å (Table 4). The Cu–S distances within the coordination tetrahedron in all the reported structures vary from 2.325(2) Å to 2.388(3) Å (Table 4).

The IR and Raman spectra of SrLnCuS<sub>3</sub> (Ln = La, Nd, Tm) each contain bands exclusively up to about 350 cm<sup>−1</sup> (Figure 2), thus the discussed compounds are both IR and Raman transparent, at least in the region of 350–4000 cm<sup>−1</sup>. The most intense bands in the IR and Raman spectra were observed at about 220–230 and 65–80 cm<sup>−1</sup>, respectively.

For SrLnCuS<sub>3</sub> (Ln = La, Nd, Tm), the experimental band gaps were obtained from the Kubelka–Munk function, and are of 1.86, 1.94 and 2.57 eV, respectively (Figure 3). Notably, the band gap values for SrLaCuS<sub>3</sub> and SrNdCuS<sub>3</sub> are similar, which might tentatively be explained by the same orthorhombic space group *Pnma* in the crystal structures of these sulfides, while the crystal structure of the discussed SrTmCuS<sub>3</sub> exhibits the orthorhombic space group *Cmcm*.

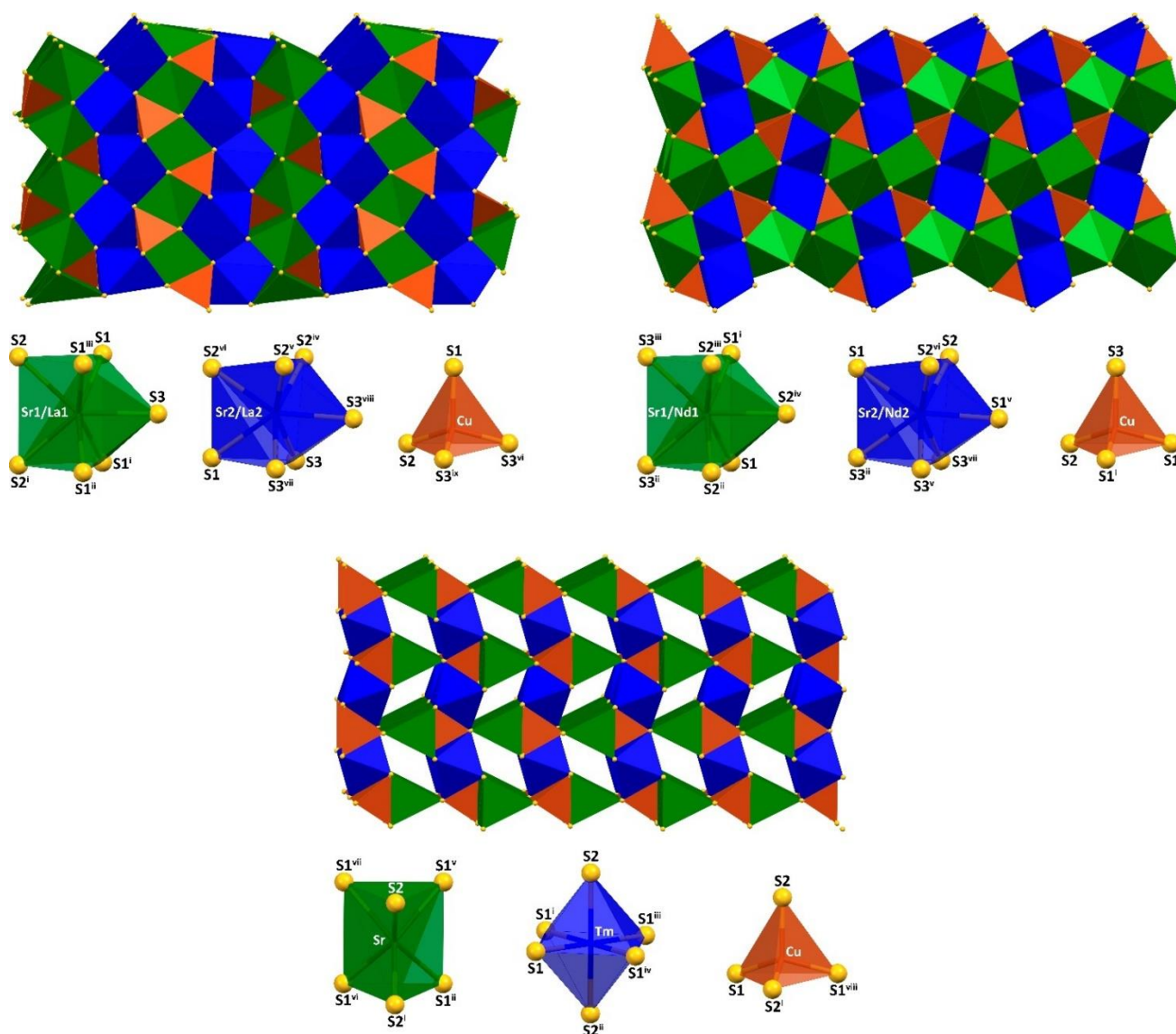


**Figure 1.** View of the crystal structures of  $\text{SrLnCu}_3$  ( $\text{Ln} = \text{La}$ , top-left;  $\text{Nd}$ , top-right,  $\text{Tm}$ , bottom) together with the coordination polyhedra formed by the metal ions. Color code: green polyhedron =  $(\text{Sr1/La1})\text{S}_7$ ,  $(\text{Sr1/Nd1})\text{S}_7$  and  $\text{SrS}_6$ ; blue polyhedron =  $(\text{Sr2/La2})\text{S}_7$ ,  $(\text{Sr2/Nd2})\text{S}_7$  and  $\text{TmS}_6$ ; burnt orange polyhedron =  $\text{CuS}_4$ . Symmetry codes for  $\text{SrLaCu}_3$ : (i)  $x, -1 + y, z$ ; (ii)  $1/2 + x, -1/2 - y, 1/2 - z$ ; (iii)  $1/2 + x, 1/2 - y, 1/2 - z$ ; (iv)  $1/2 - x, -y, -1/2 + z$ ; (v)  $1/2 - x, 1 - y, -1/2 + z$ ; (vi)  $-1/2 + x, 1/2 - y, 1/2 - z$ ; (vii)  $x, 1 + y, z$ ; (viii)  $1 - x, 1/2 + y, -z$ ; (ix)  $-1/2 + x, 1/2 - y, 1/2 - z$ . Symmetry codes for  $\text{SrNdCu}_3$ : (i)  $x, -1 + y, z$ ; (ii)  $1/2 - x, -y, 1/2 + z$ ; (iii)  $1/2 - x, -1 - y, 3/2 - z$ ; (iv)  $-1/2 + x, -1/2 - y, 3/2 - z$ ; (v)  $1/2 + x, 1/2 - y, 3/2 - z$ ; (vi)  $x, 1 + y, z$ ; (vii)  $1/2 + x, -1/2 - y, 3/2 - z$ . Symmetry codes for  $\text{SrTmCu}_3$ : (i)  $-x, -y, -z$ ; (ii)  $-x, -y, -1/2 + z$ ; (iii)  $1 + x, y, z$ ; (iv)  $1 + x, -y, -z$ ; (v)  $-1/2 - x, 1/2 + y, 1/2 - z$ ; (vi)  $-1/2 + x, 1/2 + y, z$ ; (vii)  $-3/2 - x, 1/2 + y, 1/2 - z$ ; (viii)  $-1 - x, y, 1/2 - z$ .

The field-dependent magnetic moment of both  $\text{SrNdCu}_3$  and  $\text{SrTmCu}_3$  at 296 K is linear, which is characteristic for a paramagnetic compound (Figure 4). From this dependence, the effective magnetic moment was calculated as 3.611 and 7.378  $\mu_B$  for the Nd- and Tm-based sulfides, respectively (Table 5). The temperature-dependent reciprocal magnetic susceptibility at 20–300 K is well described by the Curie–Weiss law and is the same in both the zero-field cooled (ZFC) and nonzero-field cooled (FC) modes (Figure 4). As such, the  $C$ ,  $\mu$  and  $\theta$  values were calculated for both compounds at 20–300 K (Table 5).

Experimental magnetic characteristics for SrNdCuS<sub>3</sub> and SrTmCuS<sub>3</sub> are in good agreement with the corresponding calculated parameters, obtained in the model of free ions Nd<sup>3+</sup> and Tm<sup>3+</sup>, respectively (Table 5).

**Table 4.** Bond lengths (Å) in the crystal structures of SrLnCuS<sub>3</sub> (Ln = La, Nd, Tm). For symmetry codes see Figure 1.

SrLaCuS <sub>3</sub> (Single Crystal/Powdered Sample)					
Sr1/La1–S1	2.957(1)/2.9569(11)	Sr2/La2–S1	2.996(1)/2.9988(16)	Cu–S1	2.383(1)/2.3857(18)
Sr1/La1–S1 <sup>i</sup>	2.957(1)/2.9569(11)	Sr2/La2–S2 <sup>iv</sup>	2.910(1)/2.9119(12)	Cu–S2 <sup>x</sup>	2.362(1)/2.3636(18)
Sr1/La1–S1 <sup>ii</sup>	3.003(1)/3.0036(11)	Sr2/La2–S2 <sup>v</sup>	2.910(1)/2.9119(12)	Cu–S3 <sup>vi</sup>	2.360(1)/2.3607(9)
Sr1/La1–S1 <sup>iii</sup>	3.003(1)/3.0036(11)	Sr2/La2–S2 <sup>vi</sup>	3.097(1)/3.0999(17)	Cu–S3 <sup>ix</sup>	2.360(1)/2.3607(9)
Sr1/La1–S2	3.081(1)/3.0793(13)	Sr2/La2–S3	2.964(1)/2.9627(11)		
Sr1/La1–S2 <sup>i</sup>	3.081(1)/3.0793(13)	Sr2/La2–S3 <sup>vii</sup>	2.964(1)/2.9627(11)		
Sr1/La1–S3	3.035(1)/3.0387(16)	Sr2/La2–S3 <sup>viii</sup>	3.062(1)/3.0585(16)		
SrNdCuS <sub>3</sub> (Single Crystal/Powdered Sample)					
Sr1/Nd1–S1	3.009(2)/3.002(4)	Sr2/Nd2–S1	2.944(2)/2.933(5)	Cu–S1	2.334(1)/2.335(3)
Sr1/Nd1–S1 <sup>i</sup>	3.009(2)/3.002(4)	Sr2/Nd2–S1 <sup>v</sup>	2.953(2)/2.974(5)	Cu–S1 <sup>i</sup>	2.334(1)/2.335(3)
Sr1/Nd1–S2 <sup>ii</sup>	3.036(2)/3.026(4)	Sr2/Nd2–S2	2.895(1)/2.904(4)	Cu–S2	2.325(2)/2.327(5)
Sr1/Nd1–S2 <sup>iii</sup>	3.036(2)/3.026(4)	Sr2/Nd2–S2 <sup>vi</sup>	2.895(1)/2.904(4)	Cu–S3	2.375(2)/2.388(5)
Sr1/Nd1–S2 <sup>iv</sup>	2.999(2)/2.997(5)	Sr2/Nd2–S3 <sup>ii</sup>	2.992(2)/2.980(5)		
Sr1/Nd1–S3 <sup>ii</sup>	3.136(2)/3.135(4)	Sr2/Nd2–S3 <sup>v</sup>	2.843(1)/2.851(3)		
Sr1/Nd1–S3 <sup>iii</sup>	3.136(2)/3.135(4)	Sr2/Nd2–S3 <sup>vii</sup>	2.843(1)/2.851(3)		
SrTmCuS <sub>3</sub> (Single Crystal/Powdered Sample)					
Sr–S1 <sup>ii</sup>	3.093(1)/3.093(2)	Tm–S1	2.717(1)/2.719(2)	Cu–S1	2.336(2)/2.335(3)
Sr–S1 <sup>v</sup>	3.093(1)/3.093(2)	Tm–S1 <sup>i</sup>	2.717(1)/2.719(2)	Cu–S1 <sup>viii</sup>	2.336(2)/2.335(3)
Sr–S1 <sup>vi</sup>	3.093(1)/3.093(2)	Tm–S1 <sup>iii</sup>	2.717(1)/2.719(2)	Cu–S2	2.384(2)/2.383(3)
Sr–S1 <sup>vii</sup>	3.093(1)/3.093(2)	Tm–S1 <sup>iv</sup>	2.717(1)/2.719(2)	Cu–S2 <sup>i</sup>	2.384(2)/2.383(3)
Sr–S2	2.966(2)/2.966(3)	Tm–S2	2.703(1)/2.703(2)		
Sr–S2 <sup>i</sup>	2.966(2)/2.966(3)	Tm–S2 <sup>ii</sup>	2.703(1)/2.703(2)		

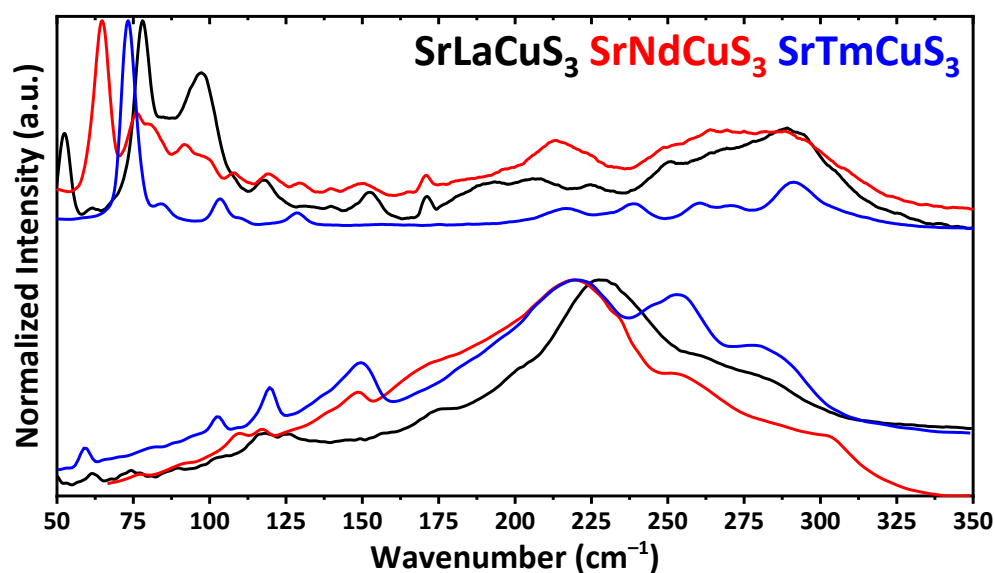


**Figure 2.** The IR (bottom) and Raman (top) spectra of SrLnCuS<sub>3</sub> (Ln = Sr, Nd, Tm).

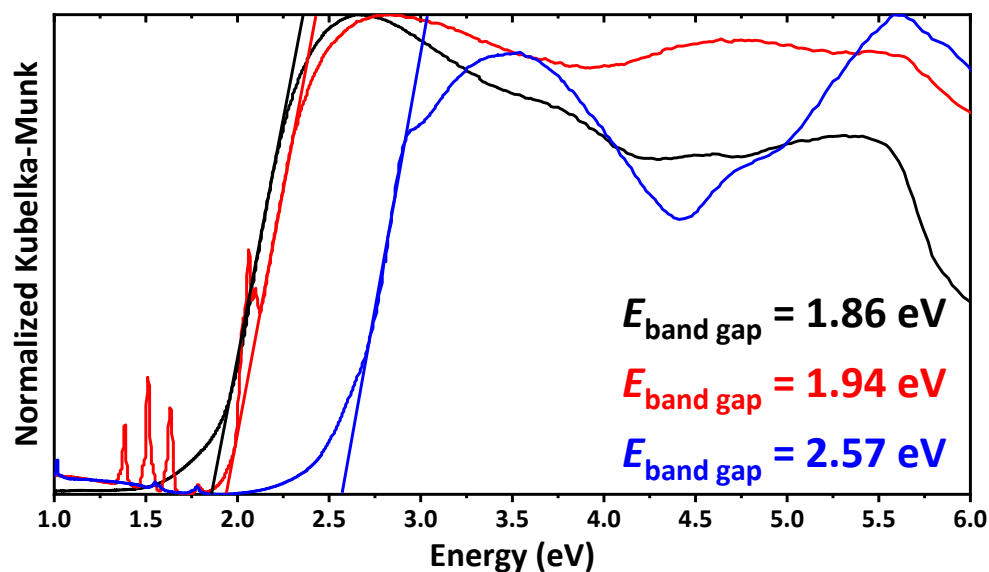


**Figure 3.** The normalized Kubelka–Munk spectra of SrLaCuS<sub>3</sub> (black), SrNdCuS<sub>3</sub> (red) and SrTmCuS<sub>3</sub> (blue). Sharp bands at about 1.30–1.80 and 2.06 in the spectrum of SrNdCuS<sub>3</sub> correspond to different transitions of Nd<sup>3+</sup> [53].

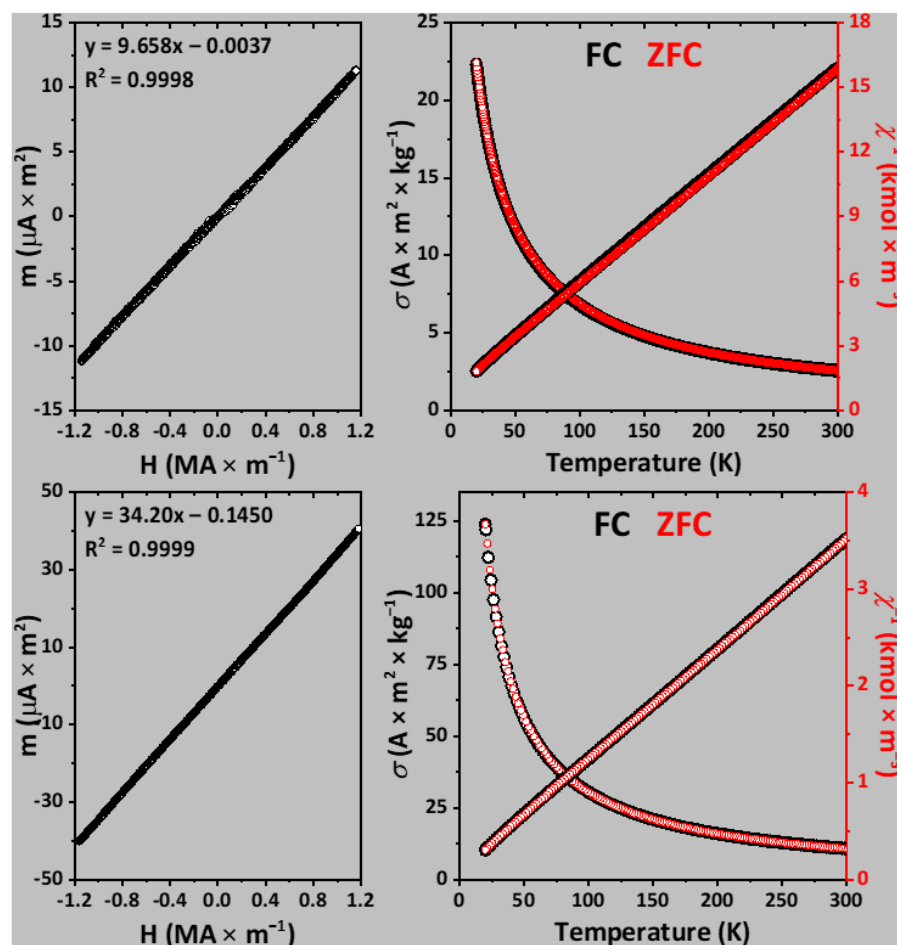


**Figure 4.** Field-dependent magnetic moments at 296 K (left), and temperature-dependent specific magnetization and reciprocal magnetic susceptibility (right) of SrNdCuS<sub>3</sub> (top) and SrTmCuS<sub>3</sub> (bottom) at 200 Oe. The temperature-dependent measurements were performed in the zero-field cooled (ZFC) and nonzero-field cooled (FC) modes.

**Table 5.** Magnetic characteristics for SrNdCuS<sub>3</sub> and SrTmCuS<sub>3</sub>.

	SrNdCuS <sub>3</sub>	SrTmCuS <sub>3</sub>
Space group	<i>Pnma</i>	<i>Cmcm</i>
Structural type	Ba <sub>2</sub> MnS <sub>3</sub>	KZrCuS <sub>3</sub>
Calculated $\mu$ ( $\mu_B$ )	3.618	7.561
Experimental $\mu_{296\text{ K}}$ ( $\mu_B$ )	3.611	7.378
Experimental $\mu_{20-300\text{ K}}$ ( $\mu_B$ )	3.52	7.57
Calculated C ( $\text{K m}^3 \text{ kmol}^{-1}$ )	0.02057	0.08983
Experimental C <sub>20-300 K</sub> ( $\text{K m}^3 \text{ kmol}^{-1}$ )	0.0195	0.0901
Experimental $\theta_{20-300\text{ K}}$ (K)	−18	−12

### 3. Materials and Methods

#### 3.1. Materials

Sr (99.2%), La (99.9%), Tm (99.9%) and CsBr (99.9%) were purchased from ChemPur (Karlsruhe, Germany). Ln<sub>2</sub>O<sub>3</sub> (Ln = La, Nd, Tm; 99.95%) were purchased from the Uralredmet manufacture (Verkhnyaya Pyshma, Russia). Cu (99.9%) was obtained from SZB Tsvetmet, OJSC (Saint Petersburg, Russia), while Cu (99.8%) was purchased from Merck (Darmstadt, Germany). S (99.5%) was purchased from Alfa Aesar (Karlsruhe, Germany). Argon (99.998%) was purchased from Kislod-Servis (Yekaterinburg, Russia). Concentrated nitric acid (extra-pure grade, 18-4 all-Union State Standard 11125-84) was purchased from Chemreaktivsnab, CJSC (Ufa, Russia). NH<sub>4</sub>SCN (98%) was obtained from Vekton Ltd. (Saint Petersburg, Russia). SrCO<sub>3</sub> (99.8%) was purchased from VitaReaktiv LLC (VitaHim Group, Dzerzhinsk, Russia).

#### 3.2. Methods

The single-crystal X-ray diffraction data for SrLaCuS<sub>3</sub> and SrTmCuS<sub>3</sub> were collected at room temperature with a Bruker–Nonius  $\kappa$ -CCD diffractometer (Mo-K $\alpha$  radiation, graphite monochromator) equipped with a CCD detector. The collected intensity data and the numerical correction of the absorption for the measured crystals were processed using the DENZO [54] and HABITUS [55] programs, respectively. The crystal structures were solved and refined using the SHELX-2013 software package [56,57].

The powder X-ray diffraction data for SrLnCuS<sub>3</sub> (Ln = La, Nd, Tm; Figure 5) were collected at room temperature with a ДРОН 7 (Burevestnik, Saint Petersburg, Russia) powder diffractometer (Cu-K $\alpha$  radiation, graphite monochromator). The step size of  $2\theta$  was 0.02°, and the counting time was 35 s per step. The lattice parameters were determined using the ITO program [58] and the crystal structures were refined by the derivative difference minimization (DDM) method [59] in the anisotropic approximation for all atoms. The effects of preferred orientation, anisotropic broadening of peak and sample surface roughness and displacement were taken into account during refinement. The data for the isostructural sulfides Ba<sub>2</sub>MnS<sub>3</sub> [60], BaLaCuS<sub>3</sub> [61] and KZrCuS<sub>3</sub> [9] were used as initial structural models for SrLaCuS<sub>3</sub>, SrNdCuS<sub>3</sub> and SrTmCuS<sub>3</sub>, respectively. The anomalous disbalance of the thermal parameters of the Sr and Ln sites after the preliminary refinement of the structures indicated a possible mixed filling of their sites due to similar ionic radii. Indeed, refinement of the occupancy of the Sr and Ln sites for the structures of SrLaCuS<sub>3</sub> and SrNdCuS<sub>3</sub> improved agreement between the calculated and experimental data as well as balanced the thermal parameters.

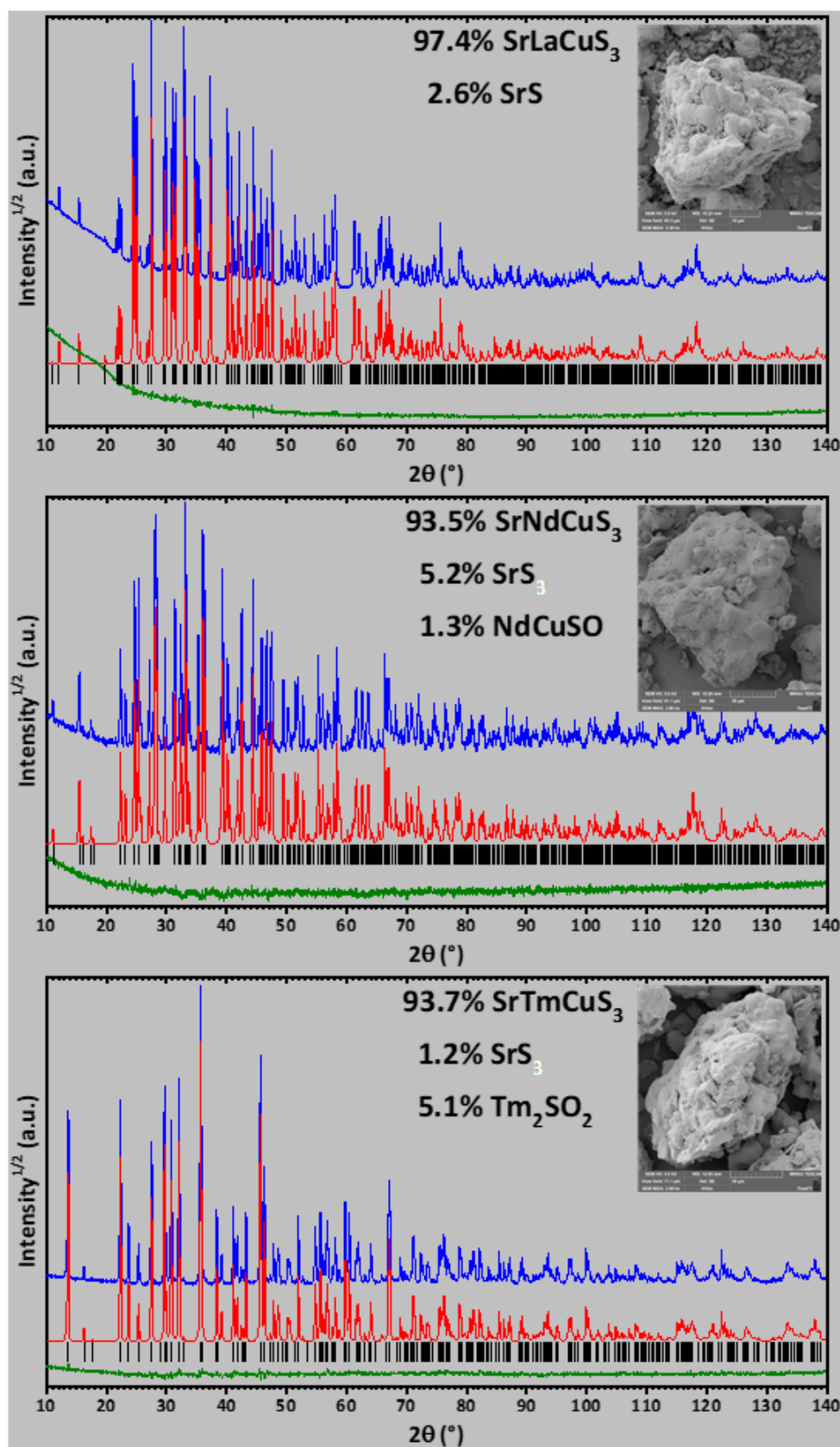


Figure 5. Observed (blue), calculated (red) and difference (green) X-ray powder diffraction patterns for SrLnCuS<sub>3</sub> after crystal structure refinement. Insets show the SEM images of SrLnCuS<sub>3</sub>.

Scanning electron microscopy (SEM) was performed on a JEOLJSM-6510 LV (JEOL Ltd., Tokyo, Japan) equipped with an energy dispersive spectrometer.

The Fourier-transform infrared (FTIR) absorption spectra in the range of 60–675  $\text{cm}^{-1}$  were recorded on a VERTEX 80v FT-IR spectrometer (Bruker OJSC, Ettlingen, Germany). The attenuated total reflectance infrared (ATR-IR) absorption spectra in the range of 400–4000  $\text{cm}^{-1}$  were recorded on a Cary 630 FTIR spectrometer (Agilent Technologies Inc., Santa Clara, CA, USA) equipped with an ATR attachment and a DTGS detector. The Raman spectra were collected in backscattering geometry using a triple monochromator Horiba JobinYvon T64000 Raman spectrometer (Horiba Ltd., Tokyo, Japan) operating in subtractive mode. The spectral resolution for the recorded Stokes-side Raman spectra was better than 3  $\text{cm}^{-1}$  (this resolution was achieved by using gratings with 1800 grooves  $\text{mm}^{-1}$  and 100  $\mu\text{m}$  slits). The single-mode radiation at 532 nm from the Spectra-Physics Excelsior laser was used as an excitation light source, the power on the sample being 5 mW.

The diffuse reflectance spectra were recorded on a UV-2600 spectrophotometer (Shimadzu OJSC, Tokyo, Japan) equipped with an ISR-2600Plus attachment with the photo-multiplier PMT of the R-928 type and InGaAs detectors.  $\text{BaSO}_4$  (99.8%) was used as a standard.

The temperature-dependent (20–300 K) magnetic susceptibilities of  $\text{SrLnCuS}_3$  (Ln = Nd, Tm) were studied on a Quantum Design MPMS3 SQUID magnetometer in a 200 Oe (15.92  $\text{kA m}^{-1}$ ) magnetic field. The measurements were performed in the zero-field cooled (ZFC) and nonzero-field cooled (FC) modes. The room temperature magnetic properties of  $\text{SrLnCuS}_3$  (Ln = Nd, Tm) were studied on a vibrating sample magnetometer with a Puzey electromagnet [62]. The magnetic field was varied in the range  $-15 \div 15$  kOe ( $-1.2 \div 1.2$  MA  $\text{m}^{-1}$ ).

### 3.3. Synthesis

Crystalline samples of  $\text{SrLnCuS}_3$  (Ln = La, Nd, Tm) in the form of single crystals were obtained from a stoichiometric ratio of the elemental strontium, copper, lanthanide and sulfur in the presence of CsBr as a flux. The reaction mixture was heated in an evacuated quartz ampoule for 8 days at 1070 °C. A thin layer of graphite was deposited on the inner wall of the quartz ampoule by a pyrolytic method to avoid side reactions with quartz glass, leading to the formation of oxosilicates. The reaction product was purified from flux residues with demineralized water. The resulting yellow needle-like crystals were suitable for a single-crystal X-ray diffraction analysis.

Powdered samples of  $\text{SrLnCuS}_3$  (Ln = La, Nd, Tm) were prepared by reductive sulfidation of the oxide mixtures in a flow of  $\text{H}_2\text{S}$  and  $\text{CS}_2$ , obtained by decomposition of ammonium thiocyanate (argon was used as a carrier gas) according to a synthetic procedure reported recently [36]. According to X-ray phase analysis, the resulting samples comprised a mixture of oxides  $\text{Ln}_2\text{O}_3$ ,  $\text{SrLnCuO}_4$ ,  $(\text{Sr,Ln})_2\text{CuO}_4$ ,  $\text{CuSrO}_2$ ,  $\text{SrLn}_2\text{O}_4$ , and  $\text{Sr}_x\text{Ln}_{2-x}\text{CuO}_4$ , which were subjected to reductive sulfidation in a flow of  $\text{H}_2\text{S}$  and  $\text{CS}_2$ , yielding the titular quaternary sulfides. Sulfidation was carried out with grinding of the resulting product in three steps: heating at 870 K for 6 h, followed by heating at 1070 K for 4 h, followed by heating at 1170 K for 20 h. This stepwise increasing of the reaction temperature is of importance to avoid the decomposition of reactor material, which, in turn, leads to the formation of silicate impurities. Thus, sulfidation is initiated by isothermal heating at 870 K until the formation of sulfides and oxysulfides, which are not so aggressive with respect to the quartz material. The sulfidation product was cooled in an argon flow. The resulting products  $\text{SrLnCuS}_3$  were examined by SEM-EDX, and the obtained data are in agreement with the powder X-ray diffraction data and are collected in Table 6.

**Table 6.** The calculated and found elemental analysis data for SrLnCuS<sub>3</sub> (Ln = La, Nd, Tm) obtained using SEM-EDX.

Compound (Mass)	Calculated (%)					Found (%)				
	Sr	Ln	Cu	S	O	Sr	Ln	Cu	S	O
SrLaCuS <sub>3</sub> (386.25)	22.68	35.96	16.45	24.90	–					
97.4% SrLaCuS <sub>3</sub> + 2.6% SrS	23.10	35.67	16.32	24.92	–	23.23	35.82	16.06	24.89	–
SrNdCuS <sub>3</sub> (391.59)	22.38	36.83	16.23	24.56	–					
93.5% SrNdCuS <sub>3</sub> + 5.2% SrS + 1.3% NdCuSO	23.02	36.40	16.04	24.49	0.06	24.68	35.18	15.52	24.54	0.08
SrTmCuS <sub>3</sub> (416.28)	21.05	40.58	15.27	23.10	–					
93.7% SrTmCuS <sub>3</sub> + 1.2% SrS + 5.1% Tm <sub>2</sub> SO <sub>2</sub>	20.18	42.60	14.45	22.36	0.40	20.53	42.51	14.25	22.30	0.41

#### 4. Conclusions

In summary, we report on a novel heterometallic quaternary sulfides SrLnCuS<sub>3</sub> (Ln = La, Nd, Tm), which were synthesized both in the form of single crystals as well as powdered samples. The former synthetic procedure allows the production of pure samples but requires heating for 8 days, while the latter synthetic approach significantly decreases the reaction time to less than 2 days. However, synthesis of the powdered samples also yields some impurities, though of minor quantities. The structures of both the single crystal and powdered samples of SrLaCuS<sub>3</sub> and SrNdCuS<sub>3</sub> belong to the orthorhombic space group *Pnma* but of different structural types, namely Ba<sub>2</sub>MnS<sub>3</sub>, BaLaCuS<sub>3</sub> and Eu<sub>2</sub>CuS<sub>3</sub>. SrTmCuS<sub>3</sub> crystallizes in the orthorhombic space group *Cmcm* with the structural type KZrCuS<sub>3</sub> for both the single crystal and powdered samples.

Three-dimensional crystal structures of the herein-obtained SrLaCuS<sub>3</sub> and SrNdCuS<sub>3</sub> are formed from the (Sr/Ln)S<sub>7</sub>-capped trigonal prisms as well as CuS<sub>4</sub> tetrahedra, however, yielding different packing of coordination polyhedra. Particularly in SrLaCuS<sub>3</sub>, alternating 2D layers are stacked, while the main backbone of the structure of SrNdCuS<sub>3</sub> is a polymeric 3D framework [(Sr/Ln)S<sub>7</sub>]<sub>n</sub>, strengthened by 1D polymeric chains (CuS<sub>4</sub>)<sub>n</sub>, with 1D channels, filled by the other Sr<sup>2+</sup>/Ln<sup>3+</sup> cations, which, in turn, form 1D dimeric ribbons. A 3D crystal structure of SrTmCuS<sub>3</sub> is constructed from the SrS<sub>6</sub> trigonal prisms, TmS<sub>6</sub> octahedra and CuS<sub>4</sub> tetrahedra. The latter two polyhedra are packed together into 2D layers, which are separated by 1D chains (SrS<sub>6</sub>)<sub>n</sub> and 1D free channels. Different crystal packings in the reported structures are, most likely, explained by both the formation of different structural types, as well as different Sr- and Ln-based coordination polyhedra. Furthermore, in both crystal structures of SrLaCuS<sub>3</sub> obtained in this work, the crystallographic positions of strontium and lanthanum are partially mixed, while only in the structure of SrNdCuS<sub>3</sub>, solved from the powder X-ray diffraction data, are the crystallographic positions of strontium and neodymium partially mixed.

The optical properties of SrLnCuS<sub>3</sub> (Ln = La, Nd, Tm) were revealed by diffuse reflectance spectroscopy, and the band gaps were found to be 1.86, 1.94 and 2.57 eV, respectively. Similar band gap values for SrLaCuS<sub>3</sub> and SrNdCuS<sub>3</sub> might tentatively be explained by the same orthorhombic space group *Pnma*.

Finally, SrNdCuS<sub>3</sub> and SrTmCuS<sub>3</sub> are paramagnetic at 20–300 K. Experimental magnetic characteristics for these sulfides are in good agreement with the corresponding calculated parameters, obtained in the model of free ions Nd<sup>3+</sup> and Tm<sup>3+</sup>, respectively.

**Author Contributions:** Conceptualization, A.V.R.; software, D.A.S.; validation, D.A.S. and A.V.R.; formal analysis, L.A.S., A.V.R., M.V.G., S.N.K., A.A.G., V.A.C. and M.A.E.; investigation, A.V.R., M.V.G., A.S.K., N.P.S., D.A.V., A.V.M. and M.A.E.; resources, A.V.R. and T.S.; data curation, A.V.R., A.S.A., T.S. and D.A.S.; writing—original draft preparation, A.V.R., A.A.G., A.S.A. and S.N.K.; writing—review and editing, A.V.R., T.S., A.A.G. and D.A.S.; visualization, A.V.R., A.A.G. and D.A.S.; project administration, A.V.R.; funding acquisition, A.V.R., M.V.G. and T.S. All authors have read and agreed to the published version of the manuscript.

**Funding:** The research was funded by the Tyumen Oblast Government, as part of the West-Siberian Interregional Science and Education Center's project No. 89-DON (3). This work was supported by state assignment of the Ministry of Science and Higher Education of the Russian Federation (Project Reg. No. 720000Φ.99.1.Б385АА13000).

**Institutional Review Board Statement:** Not applicable.

**Informed Consent Statement:** Not applicable.

**Acknowledgments:** This work was partially performed using resources of the Research Resource Center «Natural Resource Management and Physico-Chemical Research», and the laboratory for electron and probe microscopy of the Scientific and Educational Center (SEC) for Nanotechnologies (University of Tyumen). The use of the equipment of Krasnoyarsk Regional Center of Research Equipment of Federal Research Center «Krasnoyarsk Science Center SB RAS» is acknowledged.

**Conflicts of Interest:** The authors declare no conflict of interest.

## References

1. Shi, W.; Ye, J.; Zhang, Y.; Suzuki, R.; Yoshida, M.; Miyazaki, J.; Inoue, N.; Saito, Y.; Iwasa, Y. Superconductivity Series in Transition Metal Dichalcogenides by Ionic Gating. *Sci. Rep.* **2015**, *5*, 12534. [[CrossRef](#)] [[PubMed](#)]
2. Gulay, L.D.; Kaczorowski, D.; Pietraszko, A. Crystal structure and magnetic properties of YbCuPbSe<sub>3</sub>. *J. Alloys Compd.* **2006**, *413*, 26–28. [[CrossRef](#)]
3. Sturza, M.; Allred, J.M.; Malliakas, C.D.; Bugaris, D.E.; Han, F.; Chung, D.Y.; Kanatzidis, M.G. Tuning the Magnetic Properties of New Layered Iron Chalcogenides (BaF)<sub>2</sub>Fe<sub>2</sub>XQ<sub>3</sub> (Q = S, Se) by Changing the Defect Concentration on the Iron Sublattice. *Chem. Mater.* **2015**, *27*, 3280–3290. [[CrossRef](#)]
4. Ishtiyak, M.; Jana, S.; Karthikeyan, R.; Mamindla, R.; Tripathy, B.; Malladi, S.K.; Niranjana, M.; Prakash, J. Syntheses of Five New Layered Quaternary Chalcogenides SrScCuSe<sub>3</sub>, SrScCuTe<sub>3</sub>, BaScCuSe<sub>3</sub>, BaScCuTe<sub>3</sub>, and BaScAgTe<sub>3</sub>: Crystal Structures, Thermoelectric Properties, and Electronic Structures. *Inorg. Chem. Front.* **2021**, *8*, 4086–4101. [[CrossRef](#)]
5. Kuo, S.-M.; Chang, Y.-M.; Chung, I.; Jang, J.-I.; Her, B.-H.; Yang, S.-H.; Ketterson, J.B.; Kanatzidis, M.G.; Hsu, K.-F. New Metal Chalcogenides Ba<sub>4</sub>CuGa<sub>5</sub>Q<sub>12</sub> (Q = S, Se) Displaying Strong Infrared Nonlinear Optical Response. *Chem. Mater.* **2013**, *25*, 2427–2433. [[CrossRef](#)]
6. Fabini, D.H.; Koerner, M.; Seshadri, R. Candidate inorganic photovoltaic materials from electronic structure-based optical absorption and charge transport proxies. *Chem. Mater.* **2019**, *31*, 1561–1574. [[CrossRef](#)]
7. Maldonado, M.E.; Das, A.; Jawaid, A.M.; Ritter, A.J.; Vaia, R.A.; Nagaoka, D.A.; Vianna, P.G.; Seixas, L.; de Matos, C.J.S.; Baev, A.; et al. Nonlinear Optical Interactions and Relaxation in 2D Layered Transition Metal Dichalcogenides Probed by Optical and Photoacoustic Z-Scan Methods. *ACS Photonics* **2020**, *7*, 3440–3447. [[CrossRef](#)]
8. Chakraborty, S.B.; Beltran-Suito, R.; Hlukhyy, V.; Schmidt, J.; Menezes, P.W.; Driess, M. Crystalline Copper Selenide as a Reliable Non-Noble Electro(pre)catalyst for Overall Water. *ChemSusChem* **2020**, *13*, 3222–3229. [[CrossRef](#)]
9. Mansuetto, M.F.; Keane, P.M.; Ibers, J.A. Synthesis, structure, and conductivity of the new group IV chalcogenides KCuZrQ<sub>3</sub> (Q = S, Se, Te). *J. Solid State Chem.* **1992**, *101*, 257–264. [[CrossRef](#)]
10. Sutorik, A.C.; Albritton-Thomas, J.; Hogan, T.; Kannewurf, C.R.; Kanatzidis, M.G. New Quaternary Compounds Resulting from the Reaction of Copper and f-Block Metals in Molten Polychalcogenide Salts at Intermediate Temperatures. Valence Fluctuations in the Layered CsCuCeS<sub>3</sub>. *Chem. Mater.* **1996**, *8*, 751–761. [[CrossRef](#)]
11. Huang, F.Q.; Mitchell, K.; Ibers, J.A. New Layered Materials: Syntheses, Structures, and Optical and Magnetic Properties of CsGdZnSe<sub>3</sub>, CsZrCuSe<sub>3</sub>, CsUCuSe<sub>3</sub>, and BaGdCuSe<sub>3</sub>. *Inorg. Chem.* **2001**, *40*, 5123–5126. [[CrossRef](#)] [[PubMed](#)]
12. Mitchell, K.; Haynes, C.L.; McFarland, A.D.; Van Duyne, R.P.; Ibers, J.A. Tuning of Optical Band Gaps: Syntheses, Structures, Magnetic Properties, and Optical Properties of CsLnZnSe<sub>3</sub> (Ln = Sm, Tb, Dy, Ho, Er, Tm, Yb, and Y). *Inorg. Chem.* **2002**, *41*, 1199–1204. [[CrossRef](#)] [[PubMed](#)]
13. Mitchell, K.; Huang, F.Q.; McFarland, A.D.; Haynes, C.L.; Somers, R.C.; Van Duyne, R.P.; Ibers, J.A. The CsLnMSe<sub>3</sub> Semiconductors (Ln = Rare-Earth Element, Y, M = Zn, Cd, Hg). *Inorg. Chem.* **2003**, *42*, 4109–4116. [[CrossRef](#)]
14. Wakeshima, M.; Furuuchi, F.; Hinatsu, Y. Crystal structures and magnetic properties of novel rare-earth copper sulfides, EuRCuS<sub>3</sub> (R = Y, Gd–Lu). *J. Phys. Condens. Matter.* **2004**, *16*, 5503–5518. [[CrossRef](#)]
15. Mitchell, K.; Huang, F.Q.; Caspi, E.N.; McFarland, A.D.; Haynes, C.L.; Somers, R.C.; Jorgensen, J.D.; Van Duyne, R.P.; Ibers, J.A. Syntheses, structure, and selected physical properties of CsLnMnSe<sub>3</sub> (Ln = Sm, Gd, Tb, Dy, Ho, Er, Tm, Yb, Y) and AYbZnQ<sub>3</sub> (A = Rb, Cs; Q = S, Se, Te). *Inorg. Chem.* **2004**, *43*, 1082–1089. [[CrossRef](#)]
16. Yao, J.; Deng, B.; Sherry, L.J.; McFarland, A.D.; Ellis, D.E.; Van Duyne, R.P.; Ibers, J.A. Syntheses, Structure, Some Band Gaps, and Electronic Structures of CsLnZnTe<sub>3</sub> (Ln = La, Pr, Nd, Sm, Gd, Tb, Dy, Ho, Er, Tm, Y). *Inorg. Chem.* **2004**, *43*, 7735–7740. [[CrossRef](#)]
17. Selby, H.D.; Chan, B.C.; Hess, R.F.; Abney, K.D.; Dorhout, P.K. Three new phases in the K/Cu/Th/S system: KCuThS<sub>3</sub>, K<sub>2</sub>Cu<sub>2</sub>ThS<sub>4</sub>, and K<sub>3</sub>Cu<sub>3</sub>Th<sub>2</sub>S<sub>7</sub>. *Inorg. Chem.* **2005**, *44*, 6463–6469. [[CrossRef](#)]
18. Liu, Y.; Chen, L.; Wu, L.-M.; Chan, G.H.; Van Duyne, R.P. Syntheses, Crystal and Band Structures, and Magnetic and Optical Properties of New CsLnCdTe<sub>3</sub> (Ln = La, Pr, Nd, Sm, Gd–Tm, and Lu). *Inorg. Chem.* **2008**, *47*, 855–862. [[CrossRef](#)]

19. Yao, J.; Wells, D.M.; Chan, G.H.; Zeng, H.-Y.; Ellis, D.E.; Van Duyne, R.P.; Ibers, J.A. Syntheses, Structures, Physical Properties, and Electronic Properties of Some AMUQ<sub>3</sub> Compounds (A = Alkali Metal, M = Cu or Ag, Q = S or Se). *Inorg. Chem.* **2008**, *47*, 6873–6879. [[CrossRef](#)]
20. Bugaris, D.E.; Ibers, J.A. RbAuUSE<sub>3</sub>, CsAuUSE<sub>3</sub>, RbAuUTE<sub>3</sub>, and CsAuUTE<sub>3</sub>: Syntheses and structure; magnetic properties of RbAuUSE<sub>3</sub>. *J. Solid State Chem.* **2009**, *182*, 2587–2590. [[CrossRef](#)]
21. Koscielski, L.A.; Ibers, J.A. The structural chemistry of quaternary chalcogenides of the type AMM'Q<sub>3</sub>. *Z. Anorg. Allg. Chem.* **2012**, *638*, 2585–2593. [[CrossRef](#)]
22. Ruseikina, A.V.; Solovyov, L.A.; Grigoriev, M.V.; Andreev, O.V. Crystal structure variations in the series SrLnCuS<sub>3</sub> (Ln = La, Pr, Sm, Gd, Er and Lu). *Acta Cryst.* **2019**, *C75*, 584–588. [[CrossRef](#)] [[PubMed](#)]
23. Grigoriev, M.V.; Solovyov, L.A.; Ruseikina, A.V.; Aleksandrovsky, A.S.; Chernyshev, V.A.; Velikanov, D.A.; Garmonov, A.A.; Molokeev, M.S.; Oreshonkov, A.S.; Shestakov, N.P.; et al. Quaternary Selenides EuLnCuSe<sub>3</sub>: Synthesis, Structures, Properties and In Silico Studies. *Int. J. Mol. Sci.* **2022**, *23*, 1503. [[CrossRef](#)] [[PubMed](#)]
24. Pal, K.; Hua, X.; Xia, Y.; Wolverton, C. Unraveling the structure-valence-property relationships in AMM'Q<sub>3</sub> chalcogenides with promising thermoelectric performance. *ACS Appl. Energy Mater.* **2019**, *3*, 2110–2119. [[CrossRef](#)]
25. Hao, S.; Ward, L.; Luo, Z.; Ozolins, V.; Dravid, V.P.; Kanatzidis, M.G.; Wolverton, C. Design Strategy for High-Performance Thermoelectric Materials: The Prediction of Electron-Doped KZrCuSe<sub>3</sub>. *Chem. Mater.* **2019**, *31*, 3018–3024. [[CrossRef](#)]
26. Pal, K.; Xia, Y.; Shen, J.; He, J.; Luo, Y.; Kanatzidis, M.G.; Wolverton, C. Accelerated discovery of a large family of quaternary chalcogenides with very low lattice thermal conductivity. *NPJ Comput. Mater.* **2021**, *7*, 82. [[CrossRef](#)]
27. Pal, K.; Park, C.W.; Xia, Y.; Shen, J.; Wolverton, C. Scale-invariant machine-learning model accelerates the discovery of quaternary chalcogenides with ultralow lattice thermal conductivity. *NPJ Comput. Mater.* **2022**, *8*, 48. [[CrossRef](#)]
28. Pal, K.; Xia, Y.; He, J.; Wolverton, C. High thermoelectric performance in BaAgYTe<sub>3</sub> via low lattice thermal conductivity induced by bonding heterogeneity. *Phys. Rev. Mater.* **2019**, *3*, 085402. [[CrossRef](#)]
29. Matsunaga, T.; Yamada, N.; Kojima, R.; Shamoto, S.; Sato, M.; Tanida, H.; Uruga, T.; Kohara, S.; Takata, M.; Zalden, P.; et al. Phase-change materials: Vibrational softening upon crystallization and its impact on thermal properties. *Adv. Funct. Mater.* **2011**, *21*, 2232–2239. [[CrossRef](#)]
30. Biswas, K.; He, J.; Blum, I.D.; Wu, C.-I.; Hogan, T.P.; Seidman, D.N.; Dravid, V.P.; Kanatzidis, M.G. High-performance bulk thermoelectrics with all-scale hierarchical architectures. *Nature* **2012**, *489*, 414–418. [[CrossRef](#)]
31. Darolia, R. Thermal barrier coatings technology: Critical review, progress update, remaining challenges and prospects. *Int. Mater. Rev.* **2013**, *58*, 315–348. [[CrossRef](#)]
32. Zhao, L.-D.; Tan, G.; Hao, S.; He, J.; Pei, Y.; Chi, H.; Wang, H.; Gong, S.; Xu, H.; Dravid, V.P.; et al. Ultrahigh power factor and thermoelectric performance in holedoped single crystal SnSe. *Science* **2016**, *351*, 141–144. [[CrossRef](#)] [[PubMed](#)]
33. Wu, P.; Christuk, A.E.; Ibers, J.A. New Quaternary Chalcogenides BaLnMQ<sub>3</sub> (Ln = Rare Earth or Sc; M = Cu, Ag; Q = S, Se). Structure and Property Variation vs Rare-Earth Element. *J. Solid State Chem.* **1994**, *110*, 337–344. [[CrossRef](#)]
34. Ruseikina, A.V.; Andreev, O.V.; Galenko, E.O.; Koltsov, S.I. Trends in thermodynamic parameters of phase transitions of lanthanide sulfides SrLnCuS<sub>3</sub> (Ln = La–Lu). *J. Therm. Anal. Calorim.* **2017**, *128*, 993–999. [[CrossRef](#)]
35. Ruseikina, A.V.; Demchuk, Z.A. Crystal Structure and Properties of AHoCuS<sub>3</sub> (A = Sr or Eu). *Russ. J. Inorg. Chem.* **2017**, *62*, 27–32. [[CrossRef](#)]
36. Ruseikina, A.V.; Molokeev, M.S.; Chernyshev, V.A.; Aleksandrovsky, A.S.; Krylov, A.S.; Krylova, S.N.; Velikanov, D.A.; Grigoriev, M.V.; Maximov, N.G.; Shestakov, N.P.; et al. Synthesis, structure, and properties of EuScCuS<sub>3</sub> and SrScCuS<sub>3</sub>. *J. Solid State Chem.* **2021**, *296*, 121926. [[CrossRef](#)]
37. Ruseikina, A.V.; Chernyshev, V.A.; Velikanov, D.A.; Aleksandrovsky, A.S.; Shestakov, N.P.; Molokeev, M.S.; Grigoriev, M.V.; Andreev, O.V.; Garmonov, A.A.; Matigorov, A.V.; et al. Regularities of the property changes in the compounds EuLnCuS<sub>3</sub> (Ln = La–Lu). *J. Alloys Compd.* **2021**, *874*, 159968. [[CrossRef](#)]
38. Oreshonkov, A.S.; Azarapin, N.O.; Shestakov, N.P.; Adichtchev, S.V. Experimental and DFT study of BaLaCuS<sub>3</sub>: Direct band gap semiconductor. *J. Phys. Chem. Solids* **2021**, *148*, 109670. [[CrossRef](#)]
39. Zhang, S.B.; Wei, S.H.; Zunger, A.; Katayama-Yoshida, H. Defect physics of the CuInSe<sub>2</sub> chalcopyrite semiconductor. *Phys. Rev. B.* **1998**, *57*, 9642–9656. [[CrossRef](#)]
40. Contreras, M.A.; Ramanathan, K.; AbuShama, J.; Hasoon, F.; Young, D.L.; Egaas, B.; Noufi, R. Diode characteristics in state-of-the-art ZnO/CdS/Cu(In<sub>1-x</sub>Ga<sub>x</sub>)Se<sub>2</sub> solar cells. *Prog. Photovolt. Res. Appl.* **2005**, *13*, 209–216. [[CrossRef](#)]
41. Repins, I.L.; Stanbery, B.J.; Young, D.L.; Li, S.S.; Metzger, W.K.; Perkins, C.L.; Shafarman, W.N.; Beck, M.E.; Chen, L.; Kapur, V.K.; et al. Comparison of device performance and measured transport parameters in widely varying Cu(In,Ga)(Se,S) solar cells. *Prog. Photovolt. Res. Appl.* **2006**, *14*, 25–43. [[CrossRef](#)]
42. Repins, I.; Contreras, M.; Romero, M.; Yan, Y.; Metzger, W.; Li, J.; Johnston, S.; Egaas, B.; DeHart, C.; Scharf, J. Characterization of 19.9%-Efficient CIGS. In Proceedings of the 33rd IEEE Photovoltaic Specialists Conference, San Diego, CA, USA, 11–16 May 2008; Paper NREL/CP-520-42539.
43. Ruseikina, A.V.; Solov'ev, L.A.; Andreev, O.V. Crystal Structures and Properties of SrLnCuS<sub>3</sub> (Ln = La, Pr). *Russ. J. Inorg. Chem.* **2014**, *59*, 196–201. [[CrossRef](#)]
44. Ruseikina, A.V.; Solov'ev, L.A. Crystal Structures of  $\alpha$ - and  $\beta$ -SrCeCuS<sub>3</sub>. *Russ. J. Inorg. Chem.* **2016**, *61*, 482–487. [[CrossRef](#)]

45. Ruseikina, A.V.; Solov'ev, L.A.; Galenko, E.O.; Grigor'ev, M.V. Refined Crystal Structures of SrLnCuS<sub>3</sub> (Ln = Er, Yb). *Russ. J. Inorg. Chem.* **2018**, *63*, 1225–1231. [[CrossRef](#)]
46. Eberle, M.A.; Strobel, S.; Schleid, T. SrCuNdS<sub>3</sub>: A new Compound with two Different Crystal Structures. *Z. Kristallogr.* **2014**, *S34*, 139.
47. Eberle, M.A.; Schleid, T. Expanding the SrCuRES<sub>3</sub> Series with the Rare-Earth Metals Scandium and Yttrium. *Z. Kristallogr.* **2016**, *S36*, 71.
48. Ruseikina, A.V.; Andreev, O.V.; Demchuk, Z.A. Preparation of Polycrystalline Samples of the EuLnCuS<sub>3</sub> (Ln = Gd, Lu) Compounds. *Inorg. Mater.* **2016**, *52*, 537–542. [[CrossRef](#)]
49. Ruseikina, A.V.; Andreev, O.V. Phase equilibria in the Cu<sub>2</sub>S–La<sub>2</sub>S<sub>3</sub>–EuS system. *Russ. J. Inorg. Chem.* **2017**, *62*, 610–618. [[CrossRef](#)]
50. Strobel, S.; Schleid, T. Quaternary Strontium Copper (I) Lanthanoid (III) Selenides with Cerium and Praseodymium: SrCuCeSe<sub>3</sub> and SrCuPrSe<sub>3</sub>, Unequal Brother and Sister. *Z. Naturforsch.* **2004**, *B59*, 985–991. [[CrossRef](#)]
51. Strobel, S.; Schleid, T. Three structure types for strontium copper (I) lanthanide (III) selenides SrCuMSe<sub>3</sub> (M = La, Gd, Lu). *J. Alloys Compd.* **2006**, *418*, 80–85. [[CrossRef](#)]
52. Shannon, R.D. Revised effective ionic radii and systematic studies of interatomic distances in halides and chalcogenides. *Acta Crystallogr.* **1976**, *A32*, 751–767. [[CrossRef](#)]
53. Ceci-Ginistrelli, E.; Smith, C.; Pugliese, D.; Lousteau, J.; Boetti, N.G.; Clarkson, W.A.; Poletti, F.; Milanese, D. Nd-doped phosphate glass cane laser: From materials fabrication to power scaling tests. *J. Alloys Compd.* **2017**, *722*, 599–605. [[CrossRef](#)]
54. Otwinowski, Z.; Minor, W. Processing of X-ray diffraction data collected in oscillation mode. *Methods Enzymol.* **1997**, *276*, 307–326. [[PubMed](#)]
55. Herrendorf, W.; Bärnighausen, H.; Habitus, A. *Program for the Optimization of the Crystal Shape for Numerical Absorption Correction in X-SHAPE*; Universität Karlsruhe: Karlsruhe, Germany, 1993.
56. Sheldrick, G.M. *Shelxl-97: Program for the Refinement of Crystal Structures*; University of Göttingen: Göttingen, Germany, 1997.
57. Sheldrick, G.M. A short history of SHELX. *Acta Crystallogr. A* **2008**, *64*, 112–122. [[CrossRef](#)]
58. Visser, J.W. A fully automatic program for finding the unit cell from powder data. *J. Appl. Crystallogr.* **1969**, *2*, 89–95. [[CrossRef](#)]
59. Solovyov, L.A. Full-Profile refinement by derivative difference minimization. *J. Appl. Crystallogr.* **2004**, *37*, 743–749. [[CrossRef](#)]
60. Brennan, T.D.; Ibers, J.A. LaPbCuS<sub>3</sub>: Cu(I) insertion into the α-La<sub>2</sub>S<sub>3</sub> framework. *J. Solid State Chem.* **1992**, *97*, 377–382. [[CrossRef](#)]
61. Christuk, A.E.; Wu, P.; Ibers, J.A. New Quaternary Chalcogenides BaLnMQ<sub>3</sub> (Ln = Rare Earth; M = Cu, Ag; Q = S, Se): I. Structures and Grinding-Induced Phase Transition in BaLaCuQ<sub>3</sub>. *J. Solid State Chem.* **1994**, *110*, 330–336. [[CrossRef](#)]
62. Velikanov, D.A. Vibration Magnetometer. RF Pat. 2341810. 20 December 2008. Available online: <http://www.freepatent.ru/patents/2341810> (accessed on 10 July 2022).